Joule

CellPress

Article

Photo-Induced Performance Enhancement of Tantalum Nitride for Solar Water Oxidation

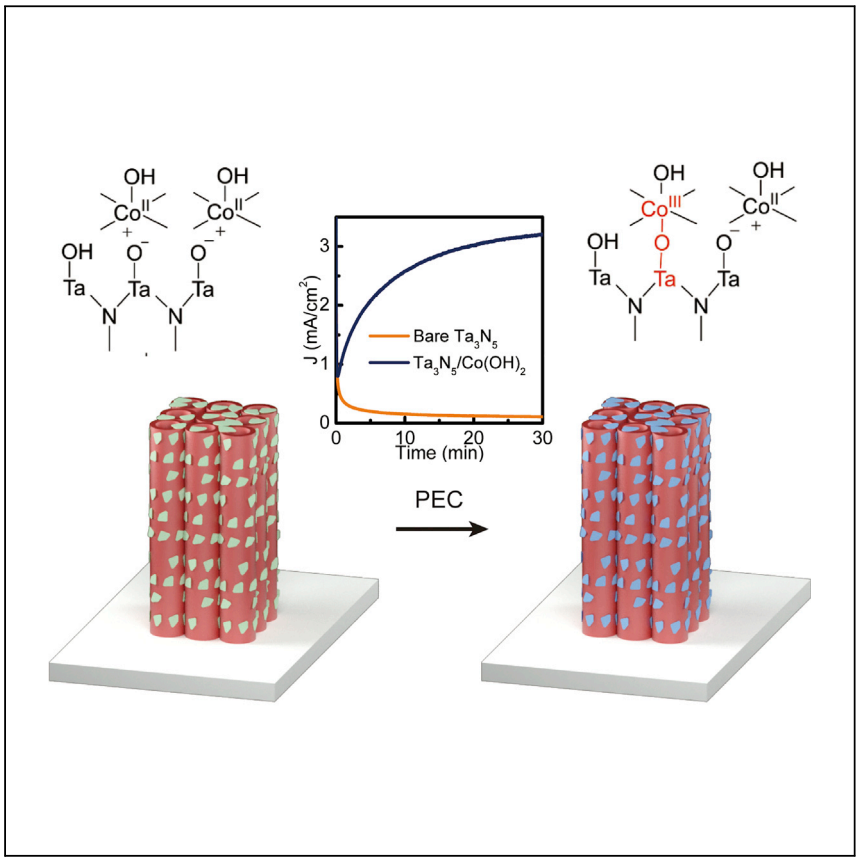

Detailed understanding of the photocatalyst/electrolyte interface is critical to further development of photocatalysts. The authors observed a unique phenomenon whereby interface reactions between Ta_3N_5 and $Co(OH)_2$ under photo-electrochemical conditions improved the performance of Ta_3N_5 for solar water oxidation. The photo-induced interface not only improved the surface kinetics but also inhibited severe Fermi-level pinning for bare Ta_3N_5. The strategy developed here sheds light on new future routes to modifying photocatalysts for better performance.

Yumin He, Peiyan Ma, Shasha Zhu, ..., Jeremy Espano, Xiahui Yao, Dunwei Wang

dunwei.wang@bc.edu

HIGHLIGHTS

$Co(OH)_2$ nanosheets improved the solar water oxidation performance of Ta_3N_5

The enhancement was unique to illumination, positive bias, and $Co(OH)_2$ catalyst

Formation of the Ta-O-Co interface improved both surface energetics and kinetics

He et al., Joule *1*, 831–842
December 20, 2017
http://dx.doi.org/10.1016/j.joule.2017.09.005

Joule

CellPress

Article

Photo-Induced Performance Enhancement of Tantalum Nitride for Solar Water Oxidation

Yumin He,[1] Peiyan Ma,[1,2] Shasha Zhu,[1] Mengdi Liu,[1] Qi Dong,[1] Jeremy Espano,[1] Xiahui Yao,[1] and Dunwei Wang[1,3,*]

SUMMARY

The semiconductor/electrolyte interface plays important roles in defining the performance of photocatalysts but is poorly studied. Here, we report a surprising observation that unique reactions at this interface under photo-electrochemical (PEC) conditions lead to unusual performance enhancement of Ta_3N_5 for solar water oxidation reactions. The enhancement was only observed when $Co(OH)_2$ was introduced as a water oxidation co-catalyst. Illumination and positive bias were also critical to the enhancement. It was proposed that $O^{\bullet}$ radical formation induced by illumination results in the formation of Ta-O-Co bonds, which exhibit less severe Fermi-level pinning when compared with Ta-O-Ta bonds that are more commonly observed on bare Ta_3N_5 under normal PEC conditions. When a high-performance oxygen evolution catalyst such as cobalt phosphate (Co-Pi) was added to the $Ta_3N_5/Co(OH)_2$ system, high photocurrent densities and good stability were achieved simultaneously.

INTRODUCTION

Photocatalysis by semiconducting materials represents an important class of chemical reactions.[1,2] Key to the functionality and performance of a photocatalyst is the interface between the semiconductor and the electrolyte.[3–5] On the one hand, the interface is critical to the separation of photogenerated charges within the semiconductor. On the other hand, the interface plays a vital role in transferring the separated charges for desired chemical reactions in the liquid electrolyte. Challenges that limit the overall performance of a photocatalyst, such as poor charge separation or low stability, are often connected to issues at the interface. For instance, previous studies on Fe_2O_3 by us[6–8] and others[9,10] have revealed that surface states at the semiconductor/liquid interface (SCLI) are a critical reason for the low photovoltages, understanding of which has led to significantly improved performance of Fe_2O_3 for solar water oxidation.[11,12] Similarly, detailed analysis on Ta_3N_5 has uncovered that rapid formation of surface states due to displacement of N atoms by O is the real reason for the fast performance degradation.[13] These previous successes highlight the importance of studying the SCLI in detail. However, most prior studies fail to account for the dynamic nature of the interface, particularly for systems where co-catalysts are present.[4,14] Given that the application of co-catalysts has been increasingly recognized as critical for complex reactions such as water oxidation[15] and CO_2 reduction,[16] it is important to correct such a deficiency. Here, we report a study focused on the interactions between the co-catalyst ($Co(OH)_2$) and the photo-active semiconductor (Ta_3N_5). It is found that only under illumination conditions does a favorable interface form, leading to continuous

Context & Scale

The semiconductor/electrolyte interface plays an important role in defining the photocatalysis reaction but is poorly understood. Here, the authors used tantalum nitride as the study platform to demonstrate how detailed understanding of the interface can influence the performance. A unique type of bonding between Ta_3N_5 and $Co(OH)_2$ in the form of Ta-O-Co under photo-electrochemical conditions was found. It led to a surprising improvement in solar water oxidation performance by Ta_3N_5, which usually exhibits rapid decay. The role of the photo-induced interface was further revealed to be 2-fold. First, it suppresses Fermi-level pinning common to the Ta_3N_5/H_2O interface due to the formation of Ta-O-Ta, which has been previously identified as the key reason for rapid performance decay. Second, the new interface was found to enhance charge transfer, leading to better charge utilization. These findings offer an opportunity to modify the photocatalyst by unique reactions on the surfaces.

improvement of the performance of Ta_3N_5. The effect is in stark contrast to bare Ta_3N_5, which would degrade rapidly under similar conditions.

We chose Ta_3N_5 as the prototypical material platform for the present study for two important reasons. First, the physical properties of Ta_3N_5 render it an appealing material choice for solar water splitting applications, including a 2.1 eV direct bandgap and suitably positioned band edge positions that straddle water reduction/oxidation potentials.[17,18] Indeed, photocurrents near the theoretical limit have been measured on Ta_3N_5 under photo-electrochemical (PEC) conditions.[19] Second, poor stability is a critical issue that limits the prospect of Ta_3N_5 as a practical photo-electrode material for solar water splitting. The large gap between the promises and the measured performance makes it significant to stabilize Ta_3N_5 under PEC water oxidation conditions.[20–23] While encouraging results have been obtained recently by the introduction of, for instance, hole storage layers[24,25] or GaN,[26] these efforts do not involve chemical reactions between Ta_3N_5 and the co-catalyst and/or the passivation layer. Our approach reported here therefore represents a new direction toward stabilizing Ta_3N_5. Our efforts are also inspired by recent observations that the performance of $BiVO_4$ can be improved by a photocharging effect.[27,28] Nevertheless, the study on $BiVO_4$ photocharging primarily focused on how the semiconductor changes in response to light. Our study reported here takes an important step forward by examining the interactions between the semiconductor and the co-catalyst.

RESULTS AND DISCUSSION

The synthesis of the Ta_3N_5 nanotube (NT) was reported previously based on an anodization-nitridation procedure.[13,29] As shown in Figure 1A, $Co(OH)_2$ was deposited on Ta_3N_5 NT using a hydrothermal method. The structure of $Co(OH)_2$ and its nanosheet morphology was confirmed using X-ray powder diffraction and scanning electron microscopy (SEM), respectively (Figures S1 and S2 in the Supplemental Information). The characteristic photocurrent density-voltage relationship (J-V) for Ta_3N_5 with $Co(OH)_2$ is plotted in Figure S3A in the Supplemental Information. It is surprising that repeated PEC scans led to an obvious increase in the photocurrent, which is opposite to how bare Ta_3N_5 photo-electrodes behave (Figure S3B). For easy comparison of the effect, the photocurrent densities at V = 1.23 V (versus reversible hydrogen electrode [RHE]) were plotted as a function of PEC scans in Figure 1B. It is seen that at the 14^{th} cycle, the photocurrent (3.1 mA/cm^2) was three times that of the first scan (1.0 mA/cm^2). The effect was also obvious from the chronoamperometry data as shown in Figure 1C, where the photocurrent densities of two samples, bare Ta_3N_5 and Ta_3N_5 with $Co(OH)_2$ co-catalyst (denoted as $Ta_3N_5/Co(OH)_2$), were recorded as a function of time. While the initial photocurrent density for the two samples were comparable (ca. 0.8 mA/cm^2), it increased to 3.2 mA/cm^2 for the sample with $Co(OH)_2$ co-catalyst and decreased to 0.1 mA/cm^2 for bare Ta_3N_5 within 30 min. While modest compared with the best photocurrent densities as reported on Ta_3N_5 recently by us and others,[13,19,26] the value is in line with those for non-optimized systems.[25,30] We highlight that the results reported here nonetheless set the stage for future optimizations. Stability up to 5 hr can be achieved for $Ta_3N_5/Co(OH)_2$, which was much better than bare Ta_3N_5 (Figure S3C). More interestingly, dark electrochemical (EC) water oxidation performance did not improve under similar electrolysis conditions. The dark current density appeared to be higher compared with that under light conditions because of the high applied potentials (2 V versus RHE for the measurements of dark currents; 1.23 V versus RHE was applied for the light current measurements). At this potential, the diode formed at

[1]Department of Chemistry, Merkert Chemistry Center, Boston College, 2609 Beacon Street, Chestnut Hill, MA 02467, USA

[2]School of Chemistry, Chemical Engineering and Life Science, Wuhan University of Technology, Wuhan, Hubei 430070, P.R. China

[3]Lead Contact

*Correspondence: dunwei.wang@bc.edu

http://dx.doi.org/10.1016/j.joule.2017.09.005

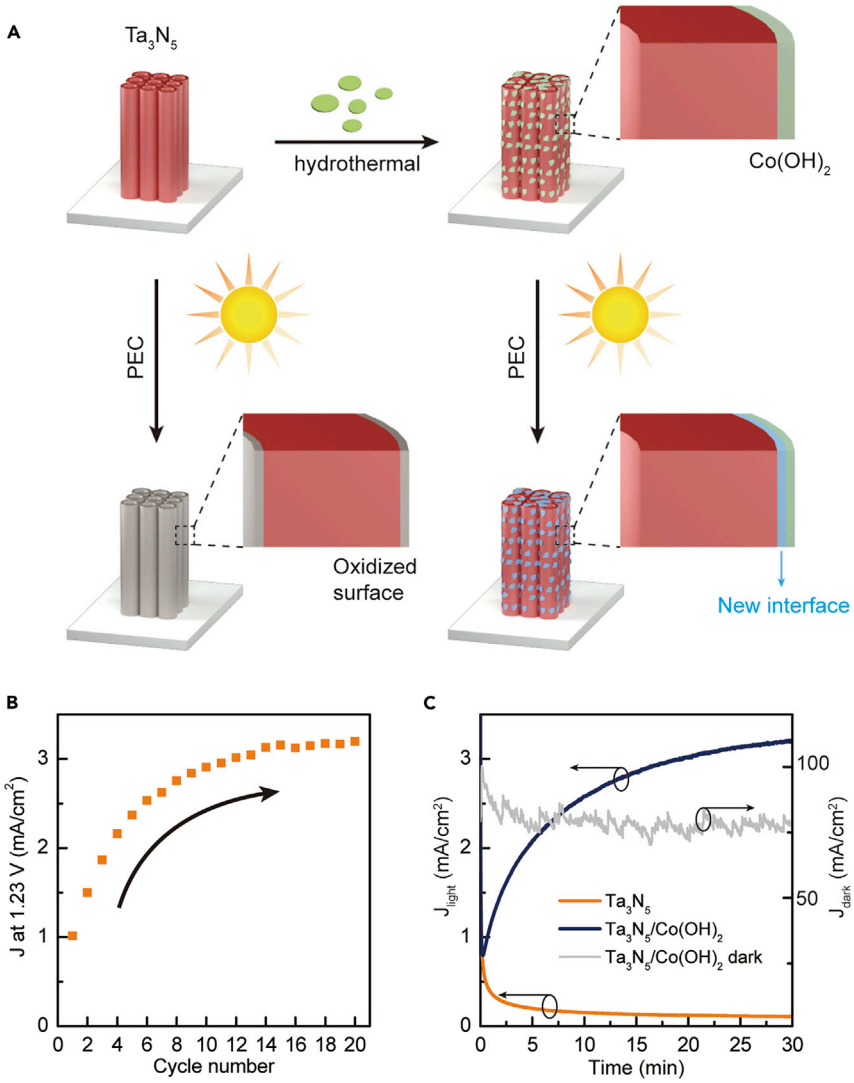

Figure 1. PEC Measurement for Ta_3N_5 and Ta_3N_5/$Co(OH)_2$

(A) Schematics illustrating the surface oxidation of bare Ta_3N_5 and the formation of new interfaces between Ta_3N_5 and $Co(OH)_2$ during solar water oxidation.

(B) Photocurrent densities at 1.23 V from 20 cycles of consecutive cyclic voltammetry (CV) scans of Ta_3N_5/$Co(OH)_2$.

(C) Photocurrent density-time data of Ta_3N_5/$Co(OH)_2$ and bare Ta_3N_5 at 1.23 V. Dark current density-time data of Ta_3N_5/$Co(OH)_2$ at 2 V. The electrolyte (1 M NaOH) and the lighting conditions (AM 1.5 illumination at 100 mW/cm^2) were the same for the data shown in (B) and (C). All voltages are relative to reversible hydrogen electrode (RHE).

the Ta_3N_5/electrolyte interface is effectively operating in the breakdown regime, acting as a conductive substrate to support $Co(OH)_2$ as an oxygen evolution reaction catalyst. To exclude the possibility that the observed increase of photocurrent was due to parasitic reactions (e.g., the oxidation of Co^{2+}) instead of water oxidation, O_2 was detected as a product during photo-electrolysis, and a faradic efficiency close to 100% was measured (Figure S4).

To understand the reasons for the performance enhancement, we inspected both the semiconductor and the co-catalyst next. The improvement of water oxidation catalysts under photo-oxidation conditions has been reported by Li et al. and was

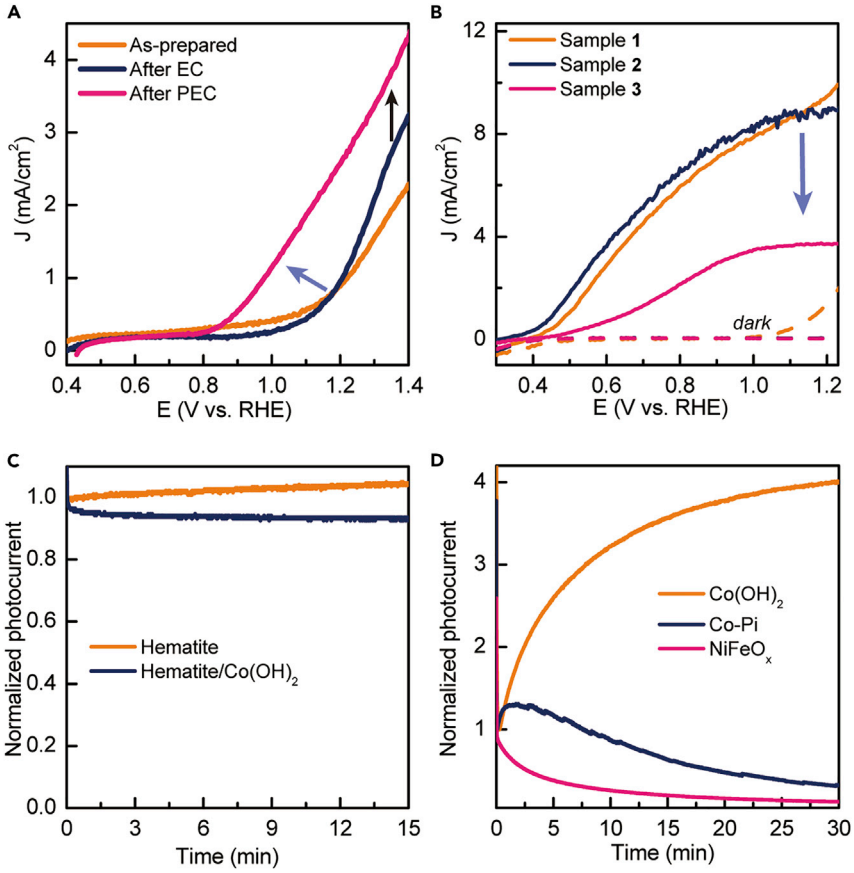

Figure 2. Control Experiments to Understand the Reasons for the Performance Enhancement

(A) J-V data of $Ta_3N_5/Co(OH)_2$ as-prepared and after EC and PEC treatment in 1 M NaOH. EC treatment, dark electrolysis at 2 V for 10 min; PEC treatment, photo-electrolysis at 1.23 V for 10 min. The arrows highlight the improvement of photocurrent densities and turn-on potentials after PEC treatments.

(B) J-V data of three different Ta_3N_5 samples in 0.1 M phosphate buffer with 0.1 M $K_4Fe(CN)_6$ (pH 10). Sample 1, as-prepared $Ta_3N_5/Co(OH)_2$; sample 2, Ta_3N_5 by dissolving $Co(OH)_2$ in $Ta_3N_5/Co(OH)_2$; sample 3, Ta_3N_5 by dissolving $Co(OH)_2$ in $Ta_3N_5/Co(OH)_2$ after PEC water oxidation. PEC water oxidation conditions: 20 consecutive CV scans from 0.4 to 1.43 V and 30 min photo-electrolysis at 1.23 V in 1 M NaOH.

The arrow highlights the decrease of photocurrent densities for Sample 3 in comparison with Samples 1 and 2.

(C) Photocurrent density-time data for hematite with and without $Co(OH)_2$ in 1 M NaOH at 1.23 V. The photocurrent was normalized to the value at the initial time.

(D) Photocurrent density-time data for Ta_3N_5 with $Co(OH)_2$, $NiFeO_x$, and Co-Pi (10 min deposition time) catalyst in 1 M NaOH at 1.23 V. The photocurrent density was normalized to the value at the initial time. The lighting conditions (AM 1.5 illumination at 100 mW/cm^2) were the same from (A) to (D).

attributed to the charging effect of $Ni(OH)_2$.[25] Similarly, EC activation of catalysts has been observed for $Co(OH)_2$ and $Ni(OH)_2$ by Boettcher et al.[31,32] To understand whether the phenomenon as shown in Figure 1 can be explained by catalyst activation, we measured and compared the J-V curves of $Ta_3N_5/Co(OH)_2$ under two different conditions: (1) after photo-electrolysis at 1.23 V for 10 min; (2) continuous electrolysis at 2 V for 10 min. As shown in Figure 2A, the photocurrent at 1.23 V increased 16% in the absence of light. By stark contrast, it increased by a of factor 2 under PEC conditions. Further increasing the applied potential and time for the EC treatment showed little enhancement for both photocurrent densities and turn-on

potentials (Figure S5). In addition, the possibility that the EC treatment will damage the photo-electrode was excluded, as shown in Figure S5. The results suggest that electrochemical activation of $Co(OH)_2$ is modest (16% only) and cannot account for the observed enhancement. Moreover, $Co(OH)_2$ was confirmed to be oxidized to CoOOH under both EC and PEC conditions (Figure S6), further supporting that changes in the catalyst were not the key reason for the performance enhancement.

Next, we conducted experiments to understand whether Ta_3N_5 was improved as a result of illumination under PEC conditions. Previously, the photocharging effect was observed on $BiVO_4$.[27,28] For this portion of the work, photo-oxidation of $Fe(CN)_6^{4-}$ instead of H_2O oxidation was employed. This is because, as a hole scavenger, $Fe(CN)_6^{4-}$ is expected to more effectively collect holes reaching the SCLI, thereby offering a reliable evaluation of the true properties of Ta_3N_5.[33–35] As shown in Figure 2B, three different samples were compared, including as-made $Ta_3N_5/Co(OH)_2$ (sample 1), bare Ta_3N_5 prepared by dissolving $Co(OH)_2$ in as-made $Ta_3N_5/Co(OH)_2$ (sample 2), and Ta_3N_5 prepared by dissolving $Co(OH)_2$ in $Ta_3N_5/Co(OH)_2$ after PEC water oxidation (sample 3). Two important observations were made. First, samples 1 and 2 exhibited similar performance. This indicates that the deposition and removal of $Co(OH)_2$ had little influence on Ta_3N_5 itself. While careful examinations of the data may reveal slight differences in the onset characteristics (better performance for sample 2), the difference is within the range of variations observed in different batches of samples. We therefore do not believe the difference to be of significance for this body of work. Second, sample 3 exhibited poorer performance than sample 2. The result was surprising because $Ta_3N_5/Co(OH)_2$ after the PEC test (but prior to the removal of $Co(OH)_2$) would exhibit better performance than sample 2 (see Figures 1 and 2A). In addition, the nanotube morphology was not changed even after the H_2SO_4 treatment, as shown in Figure S8. The results strongly support that $Co(OH)_2$ had to be present for the performance enhancement.

A third possibility that we evaluated was whether $Co(OH)_2$ co-catalyst was photo-electrochemically activated. We designed experiments to replace Ta_3N_5 with Fe_2O_3, which is a well-studied photo-electrode material that does not exhibit a photocharging effect. As shown in Figure 2C, the photocurrent of Fe_2O_3 with $Co(OH)_2$ did not increase as a result of PEC water oxidation. A small increase (<5%) in the photocurrent of the bare Fe_2O_3 sample was observed, but it is mostly likely induced by the formation of FeOOH on the surface as a more effective water oxidation catalyst than Fe_2O_3.[36] Similar conclusions (no performance enhancement upon PEC) were obtained for TiO_2 as well (Figure S9), indicating that the activation of $Co(OH)_2$ was not responsible for the performance enhancement of $Ta_3N_5/Co(OH)_2$.

The last possibility studied by this body of work was whether the effect is unique to the $Ta_3N_5/Co(OH)_2$ combination. For this purpose, we replaced $Co(OH)_2$ with other two popularly studied co-catalysts, $NiFeO_x$ and Co-Pi.[37–39] Compared with $Ta_3N_5/Co(OH)_2$, both Ta_3N_5/Co-Pi and $Ta_3N_5/NiFeO_x$ showed quick photocurrent decays during photo-electrolysis (Figure 2D) or consecutive cyclic voltammetry (CV) scans (Figures S10A and S10B). For instance, only 30% of the original photocurrent remained for Ta_3N_5/Co-Pi after 30 min photo-electrolysis. At this stage, we do not fully understand what compositions in Co-Pi prevent it from reacting with Ta_3N_5 in the same way as $Co(OH)_2$ under identical conditions, but emphasize that the results are highly reproducible (observed on over ten different batches of samples). The decay for $Ta_3N_5/NiFeO_x$ was even more severe (12% of the original photocurrent remained). However, when $Co(OH)_2$ was combined with $NiFeO_x$, a similar phenomenon as in the case of $Co(OH)_2$ could be observed, but with 30% higher photocurrent density at 1.23 V and comparable stability (Figures S10C and S10D). Furthermore,

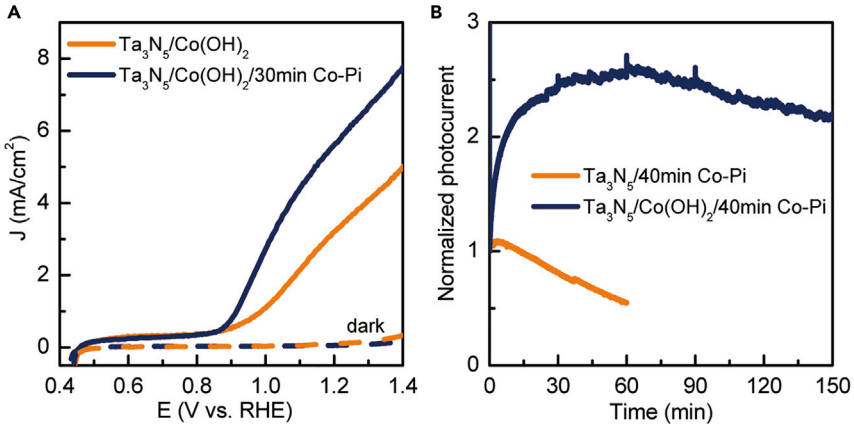

Figure 3. PEC Performance of $Ta_3N_5/Co(OH)_2$/Co-Pi

(A) J-V data of $Ta_3N_5/Co(OH)_2$ and $Ta_3N_5/Co(OH)_2$/Co-Pi after photo-electrolysis at 1.23 V for 30 min in 1 M NaOH. The deposition time of Co-Pi was 30 min.

(B) Photocurrent density-time data for Ta_3N_5/Co-Pi and $Ta_3N_5/Co(OH)_2$/Co-Pi in 1 M NaOH at 1.23 V. The deposition time of Co-Pi was 40 min. The photocurrent density was normalized to the value at the initial time. The lighting conditions (AM 1.5 illumination at 100 mW/cm^2) were the same in (A) and (B).

when $Co(OH)_2$ was combined with Co-Pi, the photocurrent density at 1.23 V could be improved to 6 mA/cm^2 (Figure 3A) with adjustment of the Co-Pi deposition time (Figure S11A). The hybrid photo-electrode showed similar stability as $Ta_3N_5/Co(OH)_2$, which was much better than that of Ta_3N_5/Co-Pi alone (Figures 3B and S11B). In addition, although the stability of Ta_3N_5/Co-Pi in Figure 3B was better than that in Figure 2D with the deposition time increased, the trend of performance decay remained the same, which further revealed the important role of the $Ta_3N_5/Co(OH)_2$ interface in good stability. It has been previously reported that different degrees of surface oxidation of Ta_3N_5 would have different influences on the properties.[19] Because the extent of surface oxidation as a function of time was similar for $Ta_3N_5/Co(OH)_2$, $Ta_3N_5/NiFeO_x$, and Ta_3N_5/Co-Pi, we concluded that such an explanation is unlikely to be responsible for the observed performance enhancement (Figure S12). Lastly, we also studied whether the observed performance enhancement was a result of the reactions between Ta_3N_5 and the precursor to $Co(OH)_2$,[40] and it was found that the effect was not dependent on the type of precursors used (Figure S13 in Supplemental Information).

To summarize the experimental observations at this point, we see that a profound performance enhancement was obtained when $Co(OH)_2$-coated Ta_3N_5 was subjected to PEC reactions. The effect was unique to the $Ta_3N_5/Co(OH)_2$ combination, and light was critical. Inspired by our previous understanding that the rapid degradation of Ta_3N_5 is due to surface Fermi-level pinning as a result of displacement of N atoms by O,[13] we assessed the surface energetics and kinetics by the open-circuit potential (OCP) and intensity modulated photocurrent spectroscopy (IMPS) techniques, respectively. Our goal was to observe whether the PEC treatment in the presence of $Co(OH)_2$ leads to reduced surface Fermi-level pinning. Indeed, as shown in Figure 4A, the OCP of $Ta_3N_5/Co(OH)_2$ as measured in light shifted negatively due to PEC reactions by 0.14 V, indicating that the surface Fermi level shifted toward the conduction band edge. The value was consistent with the change of turn-on potentials (V_{on}, Figure S3). In contrast, the OCP of bare Ta_3N_5 showed a positive shift after PEC water oxidation, indicating that the surface Fermi level has shifted

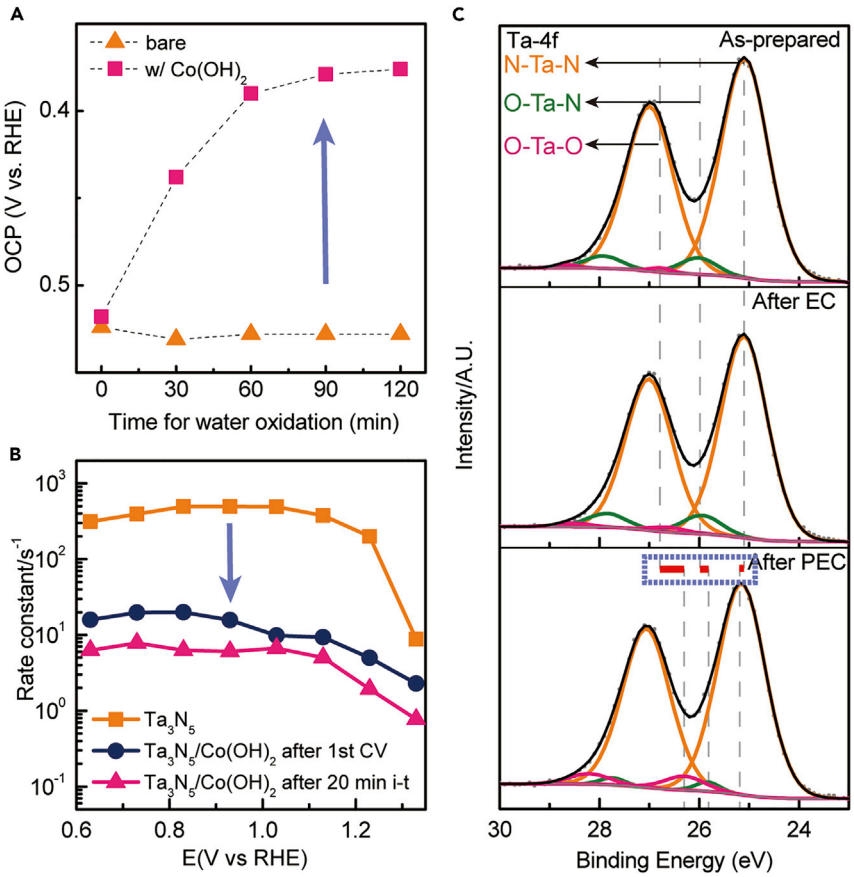

Figure 4. Detection of the Light-Induced Interface in $Ta_3N_5/Co(OH)_2$ and Its Effect on the Surface Energetics and Kinetics

(A) Open-circuit potential of bare Ta_3N_5 and $Ta_3N_5/Co(OH)_2$ with different photo-electrolysis times at 1.23 V in 1 M NaOH (AM 1.5 illumination at 100 mW/cm^2).

(B) Charge recombination rate constants of bare Ta_3N_5, $Ta_3N_5/Co(OH)_2$ after the first CV and after photoelectrolysis at 1.23 V in 1 M NaOH for 20 min (405 nm LED with 134 mW/cm^2). Detailed data interpretation is shown in Figure S15.

(C) Ta 4*f* XPS spectra of $Ta_3N_5/Co(OH)_2$ as-prepared, and after EC treatment and PEC treatment. The shifts of the individual components are highlighted in the bottom panel. EC treatment, 1.7 V in 1 M NaOH for 1 hr; PEC treatment, 1.23 V in 1 M NaOH for 30 min.

toward the valence band edge due to surface oxidation.[13] In addition, the OCP of $Ta_3N_5/Co(OH)_2$ after EC treatment was more positive than after PEC treatment, further illustrating the unique effect of light on the surface energetics (Figure S14). Taken as a whole, we clearly observed greater photovoltages by measuring the difference between the dark OCPs (Figure S14) and light OCPs (Figure 4A) owing to the suppression of the Fermi-level pinning effect.[14] Similarly, the IMPS data clearly confirmed that surface recombination rate constants (k_{rec}) at 0.9 V decreased by a factor of 3 when the PEC treatment was extended from one CV scan to 20 min photo-electrolysis (Figure 4B). Bare Ta_3N_5 featured k_{rec} values 80 times higher than those of $Ta_3N_5/Co(OH)_2$ after PEC treatment. Moreover, charge transfer kinetics was also improved after the PEC treatment, as supported by the increase in charge transfer rate constants (k_{tran}) obtained from IMPS (Figure S16) and the decrease in charge transfer resistance obtained from photo-electrochemical impedance spectroscopy (PEIS, Figure S17). We note that as an analytic tool designed to represent a simplified model with a simple photo-electrode|electrolyte

interface, IMPS has inherent deficiencies in describing complex systems such as the one studied here. As such, we caution on overinterpretation of the data in a quantitative fashion. Taken as a whole, this set of data supports that under PEC conditions, the presence of $Co(OH)_2$ on Ta_3N_5 leads to a better SCLI by not only decreasing surface recombination but also increasing charge transfer.

To further understand the origin of such an effect, we used X-ray photoelectron spectroscopy (XPS) to probe the binding energies of Ta 4*f* electrons. The data for three samples with different histories (as-prepared, after PEC treatment, and after EC treatment) are shown in Figure 3C. The peaks at 25.1 eV can be deconvoluted into three key components, including contributions from N-Ta-N, O-Ta-N, and O-Ta-O bonding. For the as-prepared sample, the binding energies of each component were consistent with the values reported in the literature.[41] The position of each component remained the same after the EC treatment. However, after the PEC treatment, the peak representing O-Ta-O bonds shifted to the negative direction by 0.4 eV (red bar highlighted in the inset of the bottom panel in Figure 4C). The peak corresponding to O-Ta-N bonds showed a similar shift but with a smaller magnitude (0.2 eV). By contrast, the peak assigned to N-Ta-N bonds shifted positively by ca. 0.1 eV, representing a shift of the surface Fermi level toward the conduction band edge. The result is consistent with the light OCP results as shown in Figure 4A. The negative shift of the O-Ta-O and O-Ta-N binding energies after PEC treatment may be explained by the interaction of Co with Ta in the form of Ta-O-Co bonding, in which case the introduction of Co weakened the neighboring Ta-O bonding, thus leading to smaller binding energies of Ta. Similar shifts of binding energies have been reported for Ti-O-Co bond formation.[42] We envision that highly surface-sensitive spectroscopic techniques such as attenuated total reflectance IR or synchrotron-enabled extended X-ray absorption fine structure spectroscopy may be used in the future to provide more details of the nature of bonding. It is noted that when $Co(OH)_2$ was removed, the binding energies of all three components (N-Ta-N, O-Ta-N, and O-Ta-O bonds) were the same as the as-prepared sample (Figure S18), providing further strong support that the $Ta_3N_5/Co(OH)_2$ combination is unique to the unusual performance enhancement observed here. In addition, the transmission electron microscopy (TEM) images also provided evidence for the formation of the $Ta_3N_5/Co(OH)_2$ interface after the PEC measurement (Figure S19).

To explain the unusual phenomenon as summarized above, we propose a mechanism as shown in Figure 5. Previous research has shown that surface oxidation of Ta_3N_5 leads to severe surface Fermi-level pinning and is the key reason for the rapid performance degradation under PEC or EC conditions (top route in Figure 5).[13,43,44] We understand that the presence of $Co(OH)_2$ promotes the formation of Ta-O-Co bonds instead of Ta-O-Ta bonds. It is nonetheless curious that such an effect was only observed when light was present. To illustrate the critical role of light, we propose that $O^{\bullet}$ radical formation under PEC conditions may be the key. As shown in Figure 5, the Ta-O-Co bonds are less likely to form under EC conditions due to the lack of $O^{\bullet}$ radicals in the absence of light.[45] To support our hypothesis, control experiments were carried out in the electrolyte with hole scavengers. It has been shown previously that the formation of $O^{\bullet}$ radical was an important step for photocatalytic water oxidation on semiconductors such as TiO_2 and TaON.[45,46] When an efficient hole scavenger was present in the electrolyte, such as $Fe(CN)_6^{4-}$, direct valence band hole transfer to solution would dominate under PEC conditions, bypassing water oxidation processes and possibly eliminating radical formation.[47] Based on this rationale, we expect that if the formation of Ta-O-Co bonds indeed

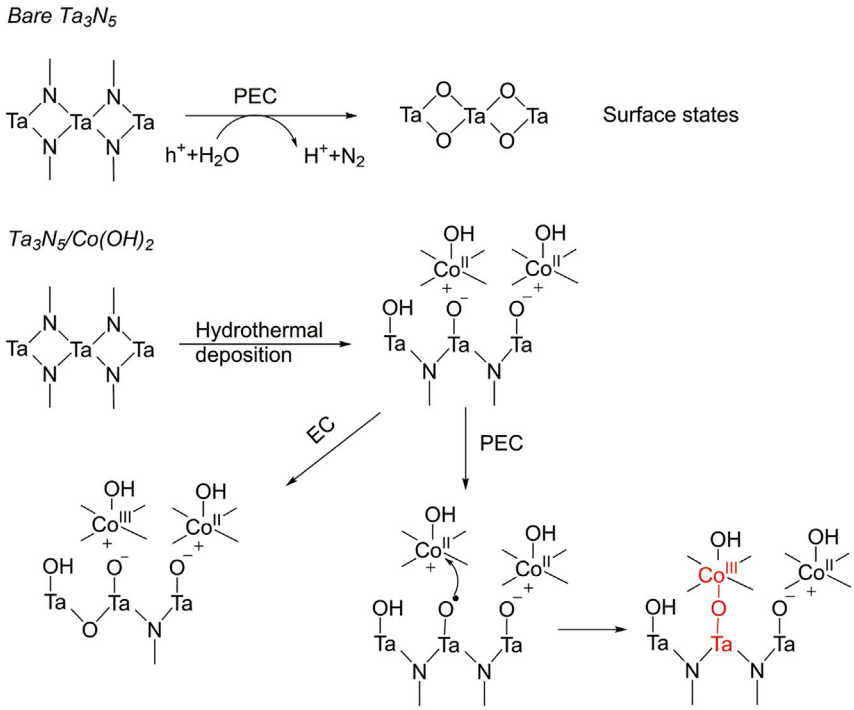

Figure 5. Proposed Mechanism for the Formation of the Ta-O-Co Bond under PEC Conditions
The surface oxidation of bare Ta_3N_5 and the electrochemical oxidation of $Ta_3N_5/Co(OH)_2$ are included for comparison.

requires $O^{\bullet}$ radical as a water oxidation intermediate, the presence of hole scavenger would inhibit its formation. Indeed, as shown in Figure S20, $Ta_3N_5/Co(OH)_2$ tested with hole scavengers showed much worse performance compared with the one without hole scavengers (1 M NaOH only) under otherwise identical PEC conditions. Nevertheless, we note that more direct evidence to support the radical-mediated interface behavior still requires the detection of the $O^{\bullet}$ radicals, and this will be a focus of our future research. For example, *in situ* electron spin resonance spectroscopy can be an effective method for this goal.[48,49]

In summary, we have observed a unique phenomenon that the water oxidation performance of $Ta_3N_5/Co(OH)_2$ photo-anode is improved under PEC conditions. The result is very different from bare Ta_3N_5, which undergoes rapid performance degradation. Experimental characterization confirmed that the effect is due to the unique chemical interactions between Ta_3N_5 and $Co(OH)_2$ in the presence of light, which leads to reduced surface Fermi-level pinning and reduction of surface charge recombination as well as the increase in surface charge transfer. $O^{\bullet}$ radical-mediated Ta-O-Co formation is proposed to explain the unusual phenomenon. In addition, with the combination of $Co(OH)_2$ as the immediate contact layer to Ta_3N_5 and another highly effective water oxidation catalyst ($NiFeO_x$ or Co-Pi) as the outer layer, both good stability and high photocurrent was achieved on Ta_3N_5.

EXPERIMENTAL PROCEDURES

Synthesis of Ta_3N_5 Nanotubes

The Ta_3N_5 NTs were synthesized through anodization of Ta foil to form tantalum oxide NTs and then annealed in NH_3 to form Ta_3N_5 based on a reported method.[13] For the anodization process, tantalum foil (0.127 mm thick; Alfa Aesar) was cut into

1 × 3.5 cm pieces with one side roughened by sandpaper for 10 min. Before the anodization, the Ta foil was cleaned by ultrasonication in acetone, methanol, isopropanol, and deionized (DI) water and dried by flowing air. The electrolyte for anodization consist of 76 mL of sulfuric acid (95%–98%; Sigma-Aldrich), 0.8 mL of hydrofluoric acid (48%; Sigma-Aldrich), and 3.2 mL of DI water after vigorous stirring. Then 60 V DC bias was applied to Ta foil against a Pt gauze counter electrode for 15 min without stirring the electrolyte. After the anodization, the sample was rinsed by ethanol and dried naturally in air. The tantalum oxide was converted to Ta_3N_5 under 1,000°C for 2 hr with anhydrous NH_3 flowing at 75 sccm (pressure was maintained at 600 torr). The synthesis of TiO_2 and hematite is described in the Supplemental Experimental Procedures.

Synthesis of Ta_3N_5/$Co(OH)_2$ Nanosheets

$Co(OH)(OCH_3)$ powders were synthesized based on a modified method.[50] Cobalt nitrate hexahydrate (0.2910 g $Co(NO_3)_2 \cdot 6H_2O$, ACS reagent, 98%; Sigma-Aldrich) was dissolved in 15 mL of methanol (99.8% ACS reagent; Sigma-Aldrich). The solution was sealed in a Teflon autoclave and placed in an oven at 180°C for 24 hr. The precipitate obtained was washed in ethanol and H_2O and collected after centrifuging for 10 min at 3,000 rpm. Pink powders were obtained after drying the precipitate in an oven at 80°C for 10 hr. A certain amount of $Co(OH)(OCH_3)$ powder was added to 10 mL of DI water and ultrasonicated for 30 min. The amount of $Co(OH)(OCH_3)$ was optimized to 2–4 mg based on the PEC performance of Ta_3N_5/$Co(OH)_2$ for water oxidation as shown in Figure S21. The supernatant was added to a Teflon autoclave with the Ta_3N_5 NT facing up, after etching in a mixture of HF:HNO_3:H_2O (1:2:7 v/v/v) for 30 s. The container was placed in an oven at 120°C for 1 hr. After that, the Ta_3N_5/$Co(OH)_2$ nanosheet sample was washed gently in DI water and dried in air. In order to remove the $Co(OH)_2$ on the Ta_3N_5 surface, the Ta_3N_5/$Co(OH)_2$ samples were etched in 1 M H_2SO_4 at 90°C for 10 min. The synthesis of another type of $Co(OH)_2$, Co-Pi, and $NiFeO_x$ is described in the Supplemental Experimental Procedures.

PEC Measurement

PEC measurement was carried out with a potentiostat (Modulab XM coupled with Modulab XM ECS software) in a three-electrode configuration. The light source was an AM 1.5 solar simulator (100 mW/cm^2, Solarlight Model 16S-300-M Air Mass Solar Simulator). For water oxidation, the electrolyte was 1 M NaOH (pH 13.6), and the reference electrode was Hg/HgO. For hole scavenger oxidation, the electrolyte was 0.1 M potassium phosphate with 0.1 M $K_4Fe(CN)_6$ (pH 10), and the reference electrode was Ag/AgCl. Particularly, the hole scavenger solution used in Figure S20 was 1 M NaOH with 0.1 M $K_4Fe(CN)_6$, and the reference electrode was Hg/HgO. In a typical CV test, the potential was swept between 0.4 V and 1.4 V at a scan rate of 20 mV/s. In a typical light OCP measurement, the open-circuit potential value was recorded after a minimum of 20 min stabilization under open-circuit conditions with vigorous stirring.

IMPS Measurement

IMPS spectra were recorded with a potentiostat (Modulab XM coupled with a frequency response analyzer, a 405 nm LED, and Modulab XM DSSC software) in the same three-electrode cell as the PEC test. The IMPS data were obtained at different applied potentials between 0.43 V and 1.63 V, and at each potential, 10% light intensity modulation was varied between 10 kHz and 0.1 Hz. The light intensity at the electrode was about 134 mW/cm^2. PEIS measurements are described in the Supplemental Experimental Procedures.

Material Characterization

The samples were imaged by a field-emission SEM (JEOL 6340F) at 10 kV and TEM (JEOL, 2010F) at 200 kV. The surface species and oxidation states were measured by XPS (K-alpha$^+$ XPS; Thermo Scientific, Al Kα = 1486.7 eV). The spectra obtained were calibrated to the binding energy of Au $4f_{7/2}$ at 84.00 eV. The Au with 1 nm thickness was sputtered onto the surface of the samples to serve as the calibration reference before the XPS measurements. The X-ray diffraction was performed on a Rigaku D/max-III A diffractometer.

SUPPLEMENTAL INFORMATION

Supplemental Information includes Supplemental Experimental Procedures and 21 figures and can be found with this article online at http://dx.doi.org/10.1016/j.joule.2017.09.005.

AUTHOR CONTRIBUTIONS

Y.H. designed and carried out the PEC measurement, material characterizations, and data analysis. P.M. synthesized the catalyst. S.Z. and M.L. helped to design and carry out the PEC measurement and nanotube synthesis. Q.D. and X.Y. collected the XPS data. J.E. helped to prepare the catalyst. D.W. directed the research. Y.H. and D.W. co-wrote the manuscript. All authors read and commented on the manuscript.

ACKNOWLEDGMENTS

The work is supported in part by the National Science Foundation (DMR 1055762 and CBET 1703663). XPS was performed at the Center for Nanoscale Systems (CNS).

Received: June 19, 2017
Revised: July 27, 2017
Accepted: September 6, 2017
Published: October 4, 2017

REFERENCES

1. Hoffmann, M.R., Martin, S.T., Choi, W., and Bahnemann, D.W. (1995). Environmental applications of semiconductor photocatalysis. Chem. Rev. *95*, 69–96.

2. Hisatomi, T., Kubota, J., and Domen, K. (2014). Recent advances in semiconductors for photocatalytic and photoelectrochemical water splitting. Chem. Soc. Rev. *43*, 7520–7535.

3. Walter, M.G., Warren, E.L., McKone, J.R., Boettcher, S.W., Mi, Q., Santori, E.A., and Lewis, N.S. (2010). Solar water splitting cells. Chem. Rev. *110*, 6446–6473.

4. Ding, C., Shi, J., Wang, Z., and Li, C. (2017). Photoelectrocatalytic water splitting: significance of cocatalysts, electrolyte and interfaces. ACS Catal. *7*, 675–688.

5. Pham, T.A., Ping, Y., and Galli, G. (2017). Modelling heterogeneous interfaces for solar water splitting. Nat. Mater. *16*, 401–408.

6. Du, C., Zhang, M., Jang, J.-W., Liu, Y., Liu, G.-Y., and Wang, D. (2014). Observation and alteration of surface states of hematite photoelectrodes. J. Phys. Chem. C *118*, 17054–17059.

7. Li, W., He, D., Sheehan, S.W., He, Y., Thorne, J.E., Yao, X., Brudvig, G.W., and Wang, D. (2016). Comparison of heterogenized molecular and heterogeneous oxide catalysts for photoelectrochemical water oxidation. Energy Environ. Sci. *9*, 1794–1802.

8. Thorne, J.E., Jang, J.-W., Liu, E.Y., and Wang, D. (2016). Understanding the origin of photoelectrode performance enhancement by probing surface kinetics. Chem. Sci. *7*, 3347–3354.

9. Klahr, B., Gimenez, S., Fabregat-Santiago, F., Bisquert, J., and Hamann, T.W. (2012). Photoelectrochemical and impedance spectroscopic investigation of water oxidation with "Co–Pi"-coated hematite electrodes. J. Am. Chem. Soc. *134*, 16693–16700.

10. Klahr, B., Gimenez, S., Fabregat-Santiago, F., Hamann, T., and Bisquert, J. (2012). Water oxidation at hematite photoelectrodes: the role of surface states. J. Am. Chem. Soc. *134*, 4294–4302.

11. Jang, J.-W., Du, C., Ye, Y., Lin, Y., Yao, X., Thorne, J., Liu, E., McMahon, G., Zhu, J., Javey, A., et al. (2015). Enabling unassisted solar water splitting by iron oxide and silicon. Nat. Commun. *6*, http://dx.doi.org/10.1038/ncomms8447.

12. Li, W., Sheehan, S.W., He, D., He, Y., Yao, X., Grimm, R.L., Brudvig, G.W., and Wang, D. (2015). Hematite-based solar water splitting in acidic solutions: functionalization by mono- and multilayers of iridium oxygen-evolution catalysts. Angew. Chem. Int. Ed. *54*, 11428–11432.

13. He, Y., Thorne, J.E., Wu, C.H., Ma, P., Du, C., Dong, Q., Guo, J., and Wang, D. (2016). What limits the performance of Ta_3N_5 for solar water splitting? Chem *1*, 640–655.

14. Thorne, J.E., Li, S., Du, C., Qin, G., and Wang, D. (2015). Energetics at the surface of photoelectrodes and its influence on the photoelectrochemical properties. J. Phys. Chem. Lett. *6*, 4083–4088.

15. Yang, X., Liu, R., He, Y., Thorne, J., Zheng, Z., and Wang, D. (2015). Enabling practical electrocatalyst-assisted photoelectrochemical water splitting with earth abundant materials. Nano Res. *8*, 56–81.

16. White, J.L., Baruch, M.F., Pander, J.E., Hu, Y., Fortmeyer, I.C., Park, J.E., Zhang, T., Liao, K.,

Gu, J., Yan, Y., et al. (2015). Light-driven heterogeneous reduction of carbon dioxide: photocatalysts and photoelectrodes. Chem. Rev. *115*, 12888–12935.

17. Morbec, J.M., Narkeviciute, I., Jaramillo, T.F., and Galli, G. (2014). Optoelectronic properties of Ta_3N_5: a joint theoretical and experimental study. Phys. Rev. B *90*, 155204.

18. Chun, W.-J., Ishikawa, A., Fujisawa, H., Takata, T., Kondo, J.N., Hara, M., Kawai, M., Matsumoto, Y., and Domen, K. (2003). Conduction and valence band positions of Ta_2O_5, TaON, and Ta_3N_5 by UPS and electrochemical methods. J. Phys. Chem. B *107*, 1798–1803.

19. Liu, G., Ye, S., Yan, P., Xiong, F.-Q., Fu, P., Wang, Z., Chen, Z., Shi, J., and Li, C. (2016). Enabling an integrated tantalum nitride photoanode to approach the theoretical photocurrent limit for solar water splitting. Energy Environ. Sci. *9*, 1327–1334.

20. Liao, M., Feng, J., Luo, W., Wang, Z., Zhang, J., Li, Z., Yu, T., and Zou, Z. (2012). Co_3O_4 nanoparticles as robust water oxidation catalysts towards remarkably enhanced photostability of a Ta_3N_5 photoanode. Adv. Funct. Mater. *22*, 3066–3074.

21. Li, Y., Zhang, L., Torres-Pardo, A., González-Calbet, J.M., Ma, Y., Oleynikov, P., Terasaki, O., Asahina, S., Shima, M., Cha, D., et al. (2013). Cobalt phosphate-modified barium-doped tantalum nitride nanorod photoanode with 1.5% solar energy conversion efficiency. Nat. Commun. *4*, http://dx.doi.org/10.1038/ncomms3566.

22. Narkeviciute, I., Chakthranont, P., Mackus, A.J.M., Hahn, C., Pinaud, B.A., Bent, S.F., and Jaramillo, T.F. (2016). Tandem core–shell Si–Ta_3N_5 photoanodes for photoelectrochemical water splitting. Nano Lett. *16*, 7565–7572.

23. Wang, L., Dionigi, F., Nguyen, N.T., Kirchgeorg, R., Gliech, M., Grigorescu, S., Strasser, P., and Schmuki, P. (2015). Tantalum nitride nanorod arrays: introducing Ni-Fe layered double hydroxides as a cocatalyst strongly stabilizing photoanodes in water splitting. Chem. Mater. *27*, 2360–2366.

24. Liu, G., Shi, J., Zhang, F., Chen, Z., Han, J., Ding, C., Chen, S., Wang, Z., Han, H., and Li, C. (2014). A tantalum nitride photoanode modified with a hole-storage layer for highly stable solar water splitting. Angew. Chem. Int. Ed. *53*, 7295–7299.

25. Liu, G., Fu, P., Zhou, L., Yan, P., Ding, C., Shi, J., and Li, C. (2015). Efficient hole extraction from a hole-storage-layer-stabilized tantalum nitride photoanode for solar water splitting. Chem. Eur. J. *21*, 9624–9628.

26. Zhong, M., Hisatomi, T., Sasaki, Y., Suzuki, S., Teshima, K., Nakabayashi, M., Shibata, N., Nishiyama, H., Katayama, M., Yamada, T., and Domen, K. (2017). Highly active GaN-stabilized Ta_3N_5 thin-film photoanode for solar water oxidation. Angew. Chem. Int. Ed. *56*, 4739–4743.

27. Li, T., He, J., Peña, B., and Berlinguette, C.P. (2016). Curing $BiVO_4$ photoanodes with ultraviolet light enhances photoelectrocatalysis. Angew. Chem. Int. Ed. *55*, 1769–1772.

28. Trzesniewski, B.J., and Smith, W.A. (2016). Photocharged $BiVO_4$ photoanodes for improved solar water splitting. J. Mater. Chem. A *4*, 2919–2926.

29. Wang, L., Nguyen, N.T., Zhou, X., Hwang, I., Killian, M.S., and Schmuki, P. (2015). Enhanced charge transport in tantalum nitride nanotube photoanodes for solar water splitting. ChemSusChem *8*, 2615–2620.

30. Grigorescu, S., So, S., Yoo, J.E., Mazare, A., Hahn, R., and Schmuki, P. (2015). Open top anodic Ta_3N_5 nanotubes for higher solar water splitting efficiency. Electrochim. Acta *182*, 803–808.

31. Trotochaud, L., Young, S.L., Ranney, J.K., and Boettcher, S.W. (2014). Nickel-iron oxyhydroxide oxygen-evolution electrocatalysts: the role of intentional and incidental iron incorporation. J. Am. Chem. Soc. *136*, 6744–6753.

32. Burke, M.S., Kast, M.G., Trotochaud, L., Smith, A.M., and Boettcher, S.W. (2015). Cobalt–iron (oxy)hydroxide oxygen evolution electrocatalysts: the role of structure and composition on activity, stability, and mechanism. J. Am. Chem. Soc. *137*, 3638–3648.

33. Ishikawa, A., Takata, T., Kondo, J.N., Hara, M., and Domen, K. (2004). Electrochemical behavior of thin Ta_3N_5 semiconductor film. J. Phys. Chem. B *108*, 11049–11053.

34. Zhong, D.K., Choi, S., and Gamelin, D.R. (2011). Near-complete Suppression of surface recombination in solar photoelectrolysis by "Co-Pi" catalyst-modified W: $BiVO_4$. J. Am. Chem. Soc. *133*, 18370–18377.

35. Cheng, Q., Fan, W., He, Y., Ma, P., Vanka, S., Fan, S., Mi, Z., and Wang, D. (2017). Photorechargeable high voltage redox battery enabled by Ta_3N_5 and GaN/Si dual-photoelectrode. Adv. Mater. *29*, http://dx.doi.org/10.1002/adma.201700312.

36. Kang, J.S., Noh, Y., Kim, J., Choi, H., Jeon, T.H., Ahn, D., Kim, J.-Y., Yu, S.-H., Park, H., Yum, J.-H., et al. (2017). Iron oxide photoelectrode with multidimensional architecture for highly efficient photoelectrochemical water splitting. Angew. Chem. Int. Ed. *56*, 6583–6588.

37. Smith, R.D.L., Prévot, M.S., Fagan, R.D., Zhang, Z., Sedach, P.A., Siu, M.K.J., Trudel, S., and Berlinguette, C.P. (2013). Photochemical route for accessing amorphous metal oxide materials for water oxidation catalysis. Science *340*, 60–63.

38. Du, C., Yang, X., Mayer, M.T., Hoyt, H., Xie, J., McMahon, G., Bischoping, G., and Wang, D. (2013). Hematite-based water splitting with low turn-on voltages. Angew. Chem. Int. Ed. *52*, 12692–12695.

39. Kanan, M.W., and Nocera, D.G. (2008). In situ formation of an oxygen-evolving catalyst in neutral water containing phosphate and Co^{2+}. Science *321*, 1072–1075.

40. Liu, Z., Ma, R., Osada, M., Takada, K., and Sasaki, T. (2005). Selective and controlled synthesis of α- and β-cobalt hydroxides in highly developed hexagonal platelets. J. Am. Chem. Soc. *127*, 13869–13874.

41. Hara, M., Chiba, E., Ishikawa, A., Takata, T., Kondo, J.N., and Domen, K. (2003). Ta_3N_5 and TaON thin films on Ta foil: surface composition and stability. J. Phys. Chem. B *107*, 13441–13445.

42. Bharti, B., Kumar, S., Lee, H.-N., and Kumar, R. (2016). Formation of oxygen vacancies and Ti^{3+} state in TiO_2 thin film and enhanced optical properties by air plasma treatment. Sci. Rep. *6*, 32355.

43. Watanabe, E., Ushiyama, H., and Yamashita, K. (2017). First-principles study of the band diagrams and Schottky-type barrier heights of aqueous Ta_3N_5 interfaces. ACS Appl. Mater. Interfaces *9*, 9559–9566.

44. Dang, H.X., Hahn, N.T., Park, H.S., Bard, A.J., and Mullins, C.B. (2012). Nanostructured Ta_3N_5 films as visible-light active photoanodes for water oxidation. J. Phys. Chem. C *116*, 19225–19232.

45. Nakamura, R., Tanaka, T., and Nakato, Y. (2005). Oxygen photoevolution on a tantalum oxynitride photocatalyst under visible-light irradiation: how does water photooxidation proceed on a metal–oxynitride surface? J. Phys. Chem. B *109*, 8920–8927.

46. Nakamura, R., and Nakato, Y. (2004). Primary intermediates of oxygen photoevolution reaction on TiO_2 (rutile) particles, revealed by in situ FTIR absorption and photoluminescence measurements. J. Am. Chem. Soc. *126*, 1290–1298.

47. Klahr, B., Gimenez, S., Fabregat-Santiago, F., Bisquert, J., and Hamann, T.W. (2012). Electrochemical and photoelectrochemical investigation of water oxidation with hematite electrodes. Energy Environ. Sci. *5*, 7626–7636.

48. Li, Z., Kong, C., and Lu, G. (2016). Visible photocatalytic water splitting and photocatalytic two-electron oxygen formation over Cu- and Fe-doped g-C_3N_4. J. Phys. Chem. C *120*, 56–63.

49. Brezová, V., Dvoranová, D., and Staško, A. (2007). Characterization of titanium dioxide photoactivity following the formation of radicals by EPR spectroscopy. Res. Chem. Intermed. *33*, 251–268.

50. Hutchings, G.S., Zhang, Y., Li, J., Yonemoto, B.T., Zhou, X., Zhu, K., and Jiao, F. (2015). In situ formation of cobalt oxide nanocubanes as efficient oxygen evolution catalysts. J. Am. Chem. Soc. *137*, 4223–4229.